**Interdisciplinary Research in Medical Sciences Specialty**
**ISSN: 3062-4401**
2025, Volume 5, Issue 2, Page No: 203-219

Available online at: www.galaxypub.co/page/journals

**Galaxy Publication**

# Gelatin–Gellan Gum–Laponite XLG Bio-ink with Enhanced Structural Stability for 3D Bioprinting Applications

**David Osei[1]*, Akua Afriyie[1], Kofi Adu[2]**

[1]Department of Bioprinting and Biomaterials Engineering, Faculty of Medicine, University of Ghana, Accra, Ghana.
[2]Department of Tissue Engineering and Bio-ink Development, Faculty of Medicine, Kwame Nkrumah University of Science and Technology, Kumasi, Ghana.

***E-mail** ✉ david.osei@ug.edu.gh

**Received:** 08 August 2025; **Revised:** 16 October 2025; **Accepted:** 23 October 2025

## ABSTRACT

Three-dimensional (3D) bioprinting constitutes a groundbreaking approach for constructing biomimetic tissue structures, holding substantial promise for tissue engineering and regenerative medicine. A key obstacle, however, lies in creating environmentally sustainable bio-inks that deliver strong printability, robust mechanical performance, and long-term stability in physiological environments, all while avoiding expensive and laborious chemical alterations. This research introduces a practical and sustainable physically crosslinked gelatin-based bio-ink, termed Gel-X, which incorporates gelatin, gellan gum, and Laponite XLG to support multi-modal bioprinting. The Gel-X formulation is assembled rapidly and simply (~1 h) by mixing the polymers in deionized water, without any chemical crosslinking agents. This results in markedly better printability, enhanced mechanical characteristics, and improved control over degradation and shape retention. The inclusion of Laponite XLG particularly reinforces the gel matrix, promoting greater structural stability and mechanical durability during extended periods. Experimental outcomes confirm that cell-laden Gel-X constructs preserve their form and strength in physiological settings, successfully countering the fast breakdown and weak mechanics common in traditional physically crosslinked bio-inks. In addition, Gel-X constructs show excellent cell compatibility, allowing the production of intricate and durable 3D architectures for bioprinting purposes. By dispensing with chemical crosslinkers, the Gel-X bio-ink represents an eco-friendly advancement for sophisticated multi-modal bioprinting. This development resolves longstanding issues in bio-ink engineering and significantly improves the reach and effectiveness of 3D bioprinting technologies.

**Keywords:** 3D bioprinting, Bio-inks, Biofabrication, Gelatin, Multi-modal printing, Sustainability

**How to Cite This Article:** Osei D, Afriyie A, Adu K. Gelatin–Gellan Gum–Laponite XLG Bio-ink with Enhanced Structural Stability for 3D Bioprinting Applications. Interdiscip Res Med Sci Spec. 2025;5(2):203-19. https://doi.org/10.51847/7CSH3toD4Z

## Introduction

Three-dimensional (3D) bioprinting has fundamentally altered the creation of tissue models that mimic natural structures, presenting important opportunities in tissue engineering and regenerative medicine (TERM) [1-4]. Through accurate layering of bio-inks containing living cells, the technology has produced sophisticated 3D constructs modeling cardiac [5-7], cartilage [8-10], corneal [11-13], lung [14-16], and skin tissues [17-19]. Principal bioprinting modalities include extrusion-based [20-22], jetting-based [23-25], and vat photopolymerization-based methods [26, 27], each providing specific benefits accompanied by distinct technical constraints. Extrusion-based methods, for instance, facilitate fast fabrication across diverse bio-ink viscosities, although they demand tight regulation of shear forces and crosslinking dynamics [28, 29]. Jetting-based techniques enable precise droplet placement of cell suspensions but necessitate strict management of shear stress, impact forces, and fluid properties [30-33]. Vat photopolymerization approaches, meanwhile, afford superior feature resolution (~20 μm) yet require fine-tuning of photo-initiator levels and light-induced reactions [34-36].

Owing to these limitations, multi-modal bioprinting strategies that combine different printing techniques have gained attention as a means to mitigate individual weaknesses and support more effective generation of complex tissues and organs. Although research in this area is still emerging, notable efforts include merging inkjet printing with electrospinning to form cartilage-resembling structures [37], employing inkjet and melt extrusion to organize cell aggregates within polymer microchambers for layered articular cartilage [38], and coupling laser-induced forward transfer (LIFT) with extrusion printing to build extensive skin equivalents for wound repair [39]. Such work demonstrates the value of multi-modal approaches in complex tissue engineering and highlights opportunities for further development and refinement.

Progress in bioprinting notwithstanding, suitable bio-inks that simultaneously provide high print fidelity, mechanical resilience, and shape stability in body-like conditions are not yet widely available [40-42]. Growing emphasis on green materials in additive manufacturing has further stimulated the search for advanced bio-ink solutions [43]. Gelatin, sourced from collagen, is a popular natural polymer due to its low cost, plentiful supply, and favorable biological interactions [44]. Used alone, however, it lacks sufficient mechanical integrity and heat resistance, leading to quick dissolution at body temperature [44]. Chemically modified variants such as gelatin methacryloyl (GelMA) were subsequently developed to overcome these drawbacks, enabling tunable stiffness through light-activated crosslinking and the formation of stable hydrogels [45]. Nevertheless, GelMA's extended synthesis requirements, dependence on photo-initiators (with potential toxicity), and sensitivity to temperature changes prior to curing reduce its convenience and affordability [46].

Gelatin's isoelectric point, which depends on extraction conditions (acid or alkaline treatment), processing temperature, and collagen source [47, 48], governs its capacity to create polyelectrolyte complexes (PECs) with polymers of opposing charge [49-51]. Type A gelatin, obtained through acid processing, retains abundant positively charged amine groups ($–NH_2$), supporting strong ionic bonding. Pairing it with negatively charged polymers such as gellan gum improves overall hydrogel stability via combined electrostatic and hydrogen-bond interactions [52, 53]. Laponite XLG, a synthetic nanosilicate with specialized surface charge properties, further strengthens these assemblies, increasing stiffness, load-bearing capacity, and resistance to collapse [54]. This material is widely applied as a rheological additive to promote shear-thinning flow and maintain printed shape fidelity [55, 56].

The current study presents a mechanically strong, physically crosslinked gelatin-based bio-ink developed specifically for extrusion-based bioprinting—a flexible and economical technique. The bio-ink combines gelatin and gellan gum (valued for its gelling ability and heat resistance) with Laponite XLG as a structural enhancer to boost mechanical performance and flow characteristics. Preparation occurs quickly (~1 h) through straightforward aqueous mixing, eliminating chemical derivatization, photo-initiators, associated costs, and toxicity risks. Crosslinking arises from ionic and hydrogen-bond networks, yielding excellent printability, thermal resistance, regulated breakdown, and sustained structural support ideal for long-term cell culture. A multi-modal printing workflow was implemented, alternating extrusion of Gel-X with jetting of cell-containing droplets in successive layers to generate complete 3D cell-laden constructs. By resolving critical shortcomings of existing materials, this bio-ink supplies a realistic, scalable option for next-generation bioprinting. The approach successfully balances affordability with performance, offering a promising route for bio-ink innovation in TERM and broader biomedical research.

## Materials and Methods

All substances and reagents applied in the present work were acquired from commercial sources. The materials included gelatin derived from porcine skin (Type A, with a gel strength of ~300 g Bloom, Sigma-Aldrich, G1890), low-acyl gellan gum (GelzanTM CM, Sigma-Aldrich, G1910), Laponite-XLG nanoclay (BYK Additives & Instruments), and sucrose (≥99.5% GC, BioXtra, Sigma-Aldrich, S7903). Deionized water with a resistivity of 18.2 MΩ was supplied by a laboratory-grade purification unit (ELGA LabWater, Purelab® flex 3). Supplementary chemicals consisted of ethyl alcohol (≥99.5%, ACS reagent, Sigma-Aldrich, 402788) and 70% isopropyl alcohol.

### *Bio-ink preparation*

The composite Gel-X bio-inks were prepared by blending gelatin powder at varying levels (6%, 9%, and 12% w/v) with Laponite-XLG nanoclay powder (1.0%, 1.5%, and 2.0% w/v), while maintaining a fixed concentration of gellan gum powder (0.25% w/v) and incorporating 0.28 M sucrose crystals. Sucrose functioned both as a

plasticizer and to preserve the bio-inks' osmolarity close to the physiological value of approximately 280 mOsm/L. The components were mixed with deionized water and stirred continuously at 60°C and 500 rpm for 1 h, resulting in the formation of the respective Gel-X formulations.

*Fourier transform infrared (FTIR) spectroscopy*

For FTIR analysis, dry powders of gelatin, low-acyl gellan gum, synthetic Laponite-XLG nanoclay, and the final composite Gel-X bio-ink were examined. Each sample (approximately 5 mg) was combined with 300 mg of potassium bromide (KBr) in an agate mortar and ground extensively to achieve uniform mixing, yielding a homogeneous fine white powder. The mixture was subsequently pressed into a disc using a KBr die under a hydraulic press at around 10 tons for 1 min. After depressurization, the transparent KBr pellet was retrieved and mounted for measurement. Spectra were collected in triplicate over the wavenumber range of 4000 $cm^{-1}$ to 400 $cm^{-1}$ with 1 $cm^{-1}$ resolution employing a ThermoFisher Scientific NicoletTM iS50 FTIR Spectrometer.

*Zeta potential and pH measurement*

Zeta (ζ) potential determinations were performed at 25°C with a Malvern Zetasizer Nano ZS (Zen 3600) using disposable folded capillary cells (DTS1070). A dilute gelatin solution (0.5% w/v) was prepared to avoid spontaneous gelation at room temperature while allowing assessment of surface charge and isoelectric point. Deionized water (refractive index 1.33) served as the dispersion medium. Solution pH was modified by adding small volumes of 0.05 mM hydrochloric acid (HCl) or 0.1 M sodium hydroxide (NaOH). pH values were verified using a portable multiparameter meter (Bante 900P) with ±0.002 pH accuracy prior to each zeta potential measurement. Five independent readings were taken for every pH condition tested.

*Rheological characterization*

Rheological evaluation of the Gel-X bio-inks was conducted on a TA Instruments Discovery Hybrid Rheometer DHR–2 fitted with a 40 mm parallel-plate geometry. A fixed sample volume of 5 was used throughout. Preliminary amplitude sweeps ensured that all subsequent tests remained inside the linear viscoelastic (LVE) domain. Steady shear viscosity was measured across shear rates from 0.1 to 1000 $s^{-1}$ (five points per decade) at a constant temperature of 25°C. Thixotropic behavior and structural recovery were studied through repeated shear-rest cycles consisting of: a low shear rate (0.1 $s^{-1}$) applied for 10 s to represent pre-printing rest, a high shear rate (500 $s^{-1}$) for 5 s to simulate extrusion conditions, and a return to 0.1 $s^{-1}$ for 5 s to mimic interlayer deposition. The full cycle was executed three times, and recovery was quantified by observing viscosity restoration following shear cessation.

*Field–emission scanning electron microscopy imaging*

Field-emission scanning electron microscopy (FE-SEM) was utilized to characterize the nanoscale architecture of the composite Gel-X bio-inks and to assess the impact of gelatin and Laponite-XLG content. Specimens were progressively dehydrated in a graded ethanol series (25%, 50%, 75%, 95%, and 100% pure ethyl alcohol, ≥99.5% ACS reagent), with 20 min incubation at each concentration. Dehydrated samples were then transferred to a critical point dryer (Leica EM CPD030, Germany) and treated with cold liquid $CO_2$ at 10°C for 2 h to safeguard the delicate 3D matrix structure. Dried constructs (n = 5) were carefully sliced with a surgical blade to expose internal cross-sections, mounted onto aluminum stubs, and sputter-coated with platinum using a Polaron SC7640 Sputter Coater (Quorum Technologies, United Kingdom). Imaging was carried out on a Carl Zeiss Ultra-Plus FE-SEM at an accelerating voltage of 2 keV with magnification up to 30,000×. Quantitative analysis of porosity and pore size distribution was performed with ImageJ software following image thresholding. Results are expressed as mean ± maximum/minimum error bars.

*Compression characterization*

Mechanical compression properties of the composite Gel-X samples were determined using an Instron 3366 Universal Testing Machine equipped with a 5 kN load cell. Cylindrical test specimens were fabricated by casting the bio-inks into circular metal molds, producing samples measuring 14 ± 0.2 mm in diameter and 5 ± 0.1 mm in height. The molded bio-inks were allowed to stabilize for 1 h at room temperature before careful demolding. Compression experiments were executed at a constant crosshead speed of 1 mm/min under standard laboratory conditions (25°C). All tests were replicated three times.

*Thermal stability and degradation studies*

Temperature-dependent stability was investigated by performing temperature ramp tests, during which the storage modulus (G′) and loss modulus (G″) were recorded from 25°C to 50°C. These measurements were taken at a fixed oscillatory frequency of 1.0 Hz and a strain of 2%, with a heating rate controlled at 2.5°C/min. Bio-inks consisting solely of gelatin (6%, 9%, and 12% w/v) were tested as reference materials to compare against the laponite-reinforced gelatin-gellan gum versions. In addition, stability at body temperature (37°C) was monitored through the damping factor (tan δ), computed as the quotient of G″ divided by G′.

For degradation assessment, the Gel-X bio-inks with different formulations were cast into circular metal molds measuring 14 mm in diameter and 5 mm in height, then left to stabilize for 1 h. After removal from the molds, the disc-shaped specimens were placed in tissue-culture treated dishes (Corning®, Sigma-Aldrich, CLS430165; 35 mm diameter × 10 mm height) and covered with 5 ml of culture medium. The constructs were incubated at 37°C for up to 14 days, with evaluations performed on Days 0, 1, 3, 7, and 14 to replicate physiological degradation conditions. At designated intervals, samples were transferred to sterile glass slides to determine the percentage alterations in mass and volume (derived from measured diameter and height). Mass was recorded using an analytical balance (Kern, ABS 220–4N) with ±0.1 mg accuracy, while dimensional changes were assessed with a Digimatic Caliper (Mitutoyo Corporation) precise to ±0.01 mm. Each time point involved five independent replicates.

*Cell culture*

Human dermal fibroblasts (HDFs) of primary origin were acquired from CellnTec Advanced Cell Systems for use in the experiments. These cells were propagated in colourless CnT-Prime Fibroblast Proliferation Medium (CnT-PR-F), consisting of a 1% serum base supplemented with defined growth factors and cofactors, and maintained at 37°C. The medium was refreshed every three days. Subculturing took place in standard tissue culture flasks at Passages 3–5; cells were detached at near-confluence (approximately 90%) with CnT Accutase cell detachment solution (CnT-Accutase 100).

*Bioprinting of 3D tissue constructs*

Bioprinting was carried out using a RegenHU Biofactory® 3D bioprinter (Switzerland) that supports both extrusion and contactless microvalve jetting print heads. Sterilization of the print heads was achieved by flushing with 70% ethanol followed by 30 min of UV irradiation. HDFs were collected and resuspended in 1× phosphate-buffered saline (PBS) (HyCloneTM, 0.0067 M, free of $Ca^{2+}$ and $Mg^{2+}$) at a density of 2 million cells/ml. To stabilize cell suspension and promote even distribution, 2% (w/v) polyvinylpyrrolidone (PVP, MW: 360 kDa) was added [57].

Extrusion printing employed 27G needles (internal diameter 210 μm), with applied pressures for the Gel-X bio-inks adjusted within the 0.5–2.5 bar range. For microvalve jetting, 100 μm nozzles were used at a steady pressure of 0.25 bar, resulting in an approximate cell deposition density of ∼8000 cells/cm² per printed layer within the multilayered constructs.

*Mechanical robustness of the 3D bioprinted tissue constructs*

A simple forceps lift test served as a qualitative measure of mechanical strength and shape fidelity for the cell-containing bioprinted constructs. During the test, the sample was carefully lifted and briefly suspended with forceps while its response to handling was observed. Observations focused on the extent of deformation (reflecting material stiffness) and the ability to retain the original geometry. The test specifically checked whether the construct could support its own weight without disintegrating, thereby indicating overall handling durability.

In addition, compressive mechanical properties of the cell-laden constructs were quantified on Day 1 and Day 3 post-fabrication using an Instron 3366 Universal Testing Machine with a 5 kN load cell. Five samples were tested per group.

*Cell viability and proliferation*

Proliferation of the embedded HDFs within the printed constructs was tracked across a 7-day incubation period at 37°C. Assessments occurred on Days 1, 3, and 7 using the PrestoBlue® cell viability reagent, which generates relative fluorescence units (RFUs) proportional to metabolic activity. Before testing, fresh medium was supplied to the constructs in 6-well plates. The PrestoBlue® solution was added at 10% of the total volume (9:1 medium-

to-reagent ratio) and allowed to incubate for 2 h at 37°C. Fluorescence signals were read on a microplate reader set at 560 nm excitation and 590 nm emission. All values were normalized relative to the Day 1 baseline to track changes in cell numbers over time. Experiments were performed in five replicates.

*Statistical analysis*

All statistical computations were based on unprocessed experimental data, which are reported as mean ± standard deviation. Comparisons among multiple groups were conducted via one-way ANOVA, with subsequent pairwise analysis using Tukey's Honestly Significant Difference (HSD) test. Levels of statistical significance are marked as $p < 0.001$ (highly significant) and $p < 0.05$ (significant).

## Results and Discussion

*Synthesis and characterization of Gel-X bio-inks*

Gelatin, an amphoteric macromolecule carrying both cationic and anionic groups, represents an attractive base material for the formulation of polyelectrolyte bio-inks. Gellan gum, a negatively charged polysaccharide, possesses deprotonated carboxylate moieties that facilitate ionic interactions. Electrostatic attractions between the oppositely charged segments of gelatin and gellan gum, supplemented by hydrogen bonding involving amide, carboxyl, and hydroxyl (–OH) groups, lead to the assembly of a cohesive hydrogel network that provides structural coherence. The incorporation of Laponite XLG, a synthetic nanosilicate clay, further augments the mechanical characteristics and overall stability of the gelatin-gellan gum system. Its disc-like morphology enables nanoscale reinforcement by inserting between polymer chains, thereby increasing rigidity and resistance to deformation. The amphoteric nature of Laponite XLG—featuring negatively charged faces and weakly positively charged rims—allows for electrostatic associations with both the positively charged domains of gelatin and the negatively charged groups of gellan gum. These interactions generate supplementary crosslinking sites, strengthening the matrix. Gelatin chains adsorb onto the Laponite surfaces via ionic and hydrogen-bond forces, while gellan gum engages similarly, yielding a denser and more resilient hydrogel architecture **(Figure 1a)**. Sucrose was included as an essential additive to sustain physiological osmolarity near 280 mOsm/L, thereby safeguarding cell function against osmotic stress. In addition to its osmoprotective role, sucrose functions as a plasticizer that weakens interchain hydrogen bonds, increasing segmental mobility, improving pliability, and minimizing the likelihood of crack formation or structural failure in the Gel-X bio-inks.

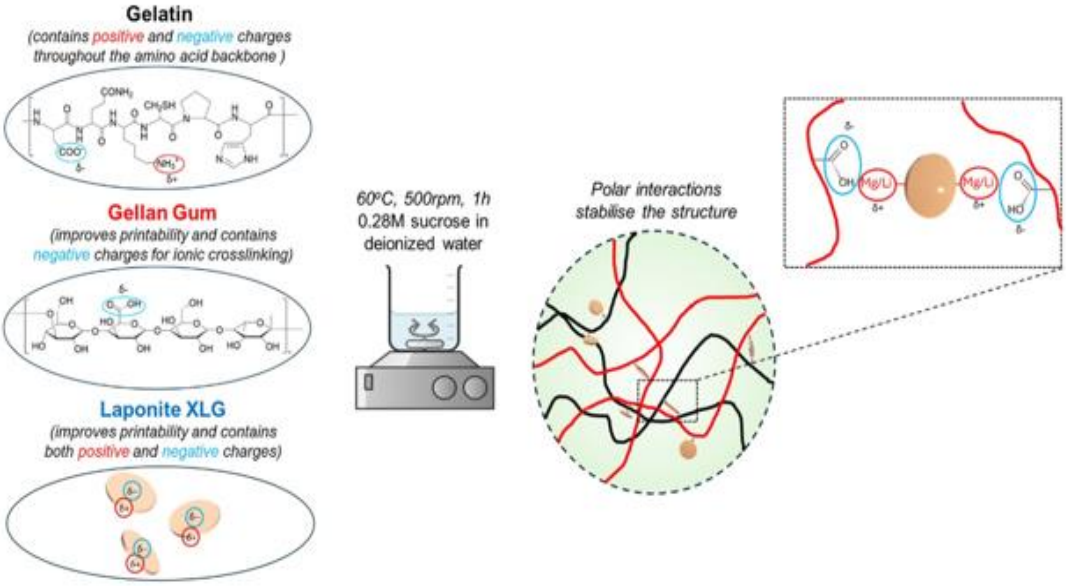


a)

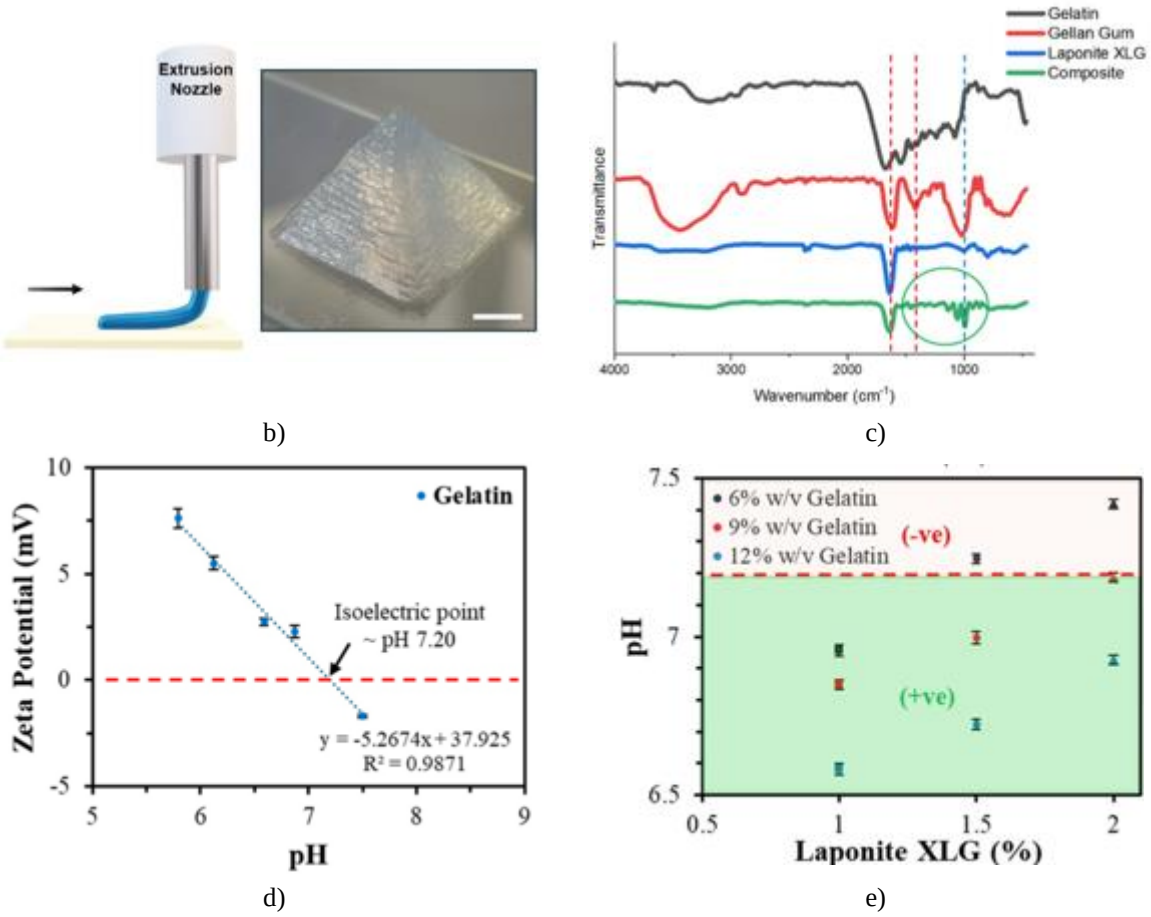


**Figure 1.** (a) Schematic representation of intermolecular associations within the bio-inks. Laponite XLG nanoclay, displaying negatively charged faces and weakly positively charged edges, forms electrostatic linkages with positively charged gelatin (black lines) and negatively charged gellan gum (red lines). These connections create extra crosslinking junctions that bolster matrix cohesion through enhanced ionic interactions and chain entanglement. (b) Fabrication of pyramid-shaped constructs from physically crosslinked composite gelatin-based (Gel-X) bio-inks exhibiting shear-thinning and thixotropic characteristics, scale bars = 5 mm. (c) FTIR spectra of individual bio-ink constituents. (d) ζ potential profile of gelatin as a function of pH for isoelectric point determination and (e) pH values of bio-ink preparations in relation to gelatin and Laponite XLG content – green and beige areas denote regions of net positive and net negative ζ potential for gelatin, respectively.

The developed Gel-X bio-inks exhibited excellent printability, surpassing many standard formulations with respect to accuracy, shape retention, and mechanical coherence. Intricate multilayered constructs, such as pyramids measuring 15 × 15 × 15 mm, were produced successfully without notable deformation or structural failure during deposition **(Figure 1b)**. Structural fidelity was preserved across successive layers owing to the complementary contributions of gelatin, gellan gum, Laponite XLG, and sucrose, which together establish a strong yet adaptable polymeric framework. Laponite XLG notably improves shear-thinning behavior, facilitating effortless flow through the nozzle during extrusion while enabling rapid viscosity recovery after deposition to prevent layer spreading. The formulations also displayed strong interlayer bonding and limited dimensional contraction, attributes essential for maintaining high resolution in sophisticated designs. Collectively, these mechanical and rheological attributes render the Gel-X bio-inks appropriate for both basic and highly elaborate bioprinting tasks.

**Figure 1c** presents the FTIR spectra of gelatin, gellan gum, Laponite XLG nanoclay, and the composite Gel-X bio-inks recorded between 4000 and 400 $cm^{-1}$. Gelatin displays multiple absorption bands in the 1800–1000 $cm^{-1}$ region arising from its varied functional groups. Gellan gum shows distinctive carboxylate ($COO^-$) stretching vibrations at approximately 1650 $cm^{-1}$ and 1400 $cm^{-1}$, whereas Laponite XLG exhibits a prominent Si–O–Si

stretching band near 1000 $cm^{-1}$. In the composite spectra, attenuation of gelatin and gellan gum peaks indicates network formation through crosslinking, while the Laponite signal remains distinct. Additional features in the fingerprint region (<1500 $cm^{-1}$) point to C–O and N–O interactions. The "house of cards" arrangement characteristic of Laponite XLG is believed to contribute to the thermal resilience of the composite matrices.

The surface charge of gelatin is governed by its isoelectric point, which varies with origin, amino acid profile, and manufacturing conditions. ζ potential measurements performed on porcine skin-derived Type A gelatin across a pH gradient revealed a progressive decline in surface charge with rising pH, yielding an isoelectric point near pH 7.20 **(Figure 1d)**. This value aligns with the manufacturer's specified range (7.0–9.5) and findings from prior research employing gelatin from the same source [58].

Physically crosslinked Gel-X bio-inks were synthesized by dissolving gelatin (G) at 6%, 9%, and 12% (w/v), Laponite XLG (X) at 1.0%, 1.5%, and 2.0% (w/v), a constant 0.25% (w/v) gellan gum, and 0.28 M sucrose in deionized water under stirring at 60°C for 1 h. The net charge of gelatin within these mixtures is strongly pH-dependent. Below the isoelectric point (pH 7.20), protonation of amine groups ($–NH_2$) confers a net positive charge; above this pH, deprotonation of carboxyl groups ($–COO^-$) results in a net negative charge. Dissolution of Laponite XLG releases hydroxide ions ($OH^-$), thereby elevating the pH of the system [59]. Experimental pH measurements showed that increasing gelatin content decreased pH, whereas higher Laponite XLG concentrations raised it **(Figure 1e)**. Overall, most Gel-X formulations exhibited a net positive charge, with the exceptions of 1.5X6G and 2X6G, which displayed net negative charges.

*Rheological analysis of Gel-X bio-inks*

The addition of Laponite XLG nanoclay is known to improve the flow characteristics of bio-inks, primarily through its pronounced shear-thinning and thixotropic responses. At rest, Laponite XLG forms a gel-like structure that transforms into a low-viscosity fluid when subjected to shear forces. This property is highly beneficial for extrusion-based bioprinting, permitting easy passage through the nozzle while enabling swift structural reformation once the material is deposited. In the current investigation, all nine Gel-X formulations displayed acceptable printability, although the pressures required varied according to their composition. Mixtures containing elevated levels of gelatin or Laponite XLG generally demanded higher extrusion pressures owing to greater viscosity. Printing pressures ranged between 0.25 and 3.5 bars as follows: 1X6G (0.50–1.00 bars), 1X9G (0.75–1.50 bars), 1×12G (1.00–2.00 bars), 1.5X6G (0.50–1.00 bars), 1.5X9G (0.75–1.50 bars), 1.5×12G (1.00–2.00 bars), 2X6G (0.25–0.50 bars), 2X9G (1.00–1.50 bars), and 2×12G (2.50–3.50 bars).

Rheological measurements verified pronounced shear-thinning across a broad shear rate spectrum (0.1–1000 $s^{-1}$) for every formulation **(Figures 2a–2c)**, consistent with the shear conditions typically encountered in extrusion bioprinting. This shear-thinning effect became especially evident at elevated shear rates exceeding 500 $s^{-1}$ (Supporting Information S1). Moreover, the Gel-X bio-inks possessed substantial yield stress and demonstrated fast viscosity restoration after shear cessation, as confirmed by thixotropic testing. Such attributes are essential for reliable extrusion, prevention of layer spreading, and preservation of geometric accuracy in printed constructs.

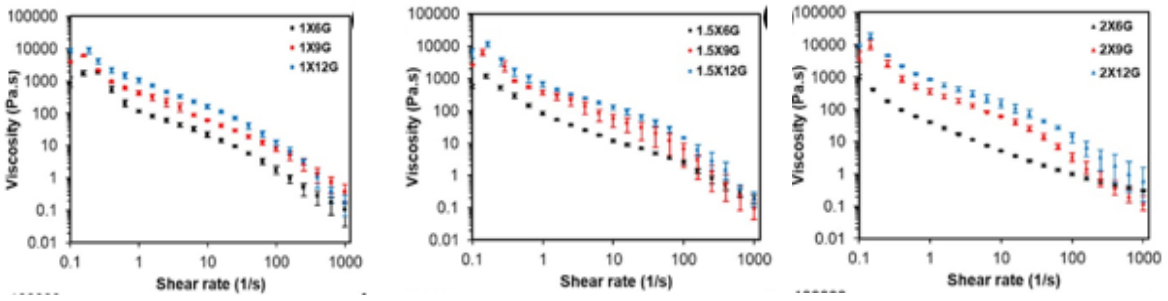


a) b) c)

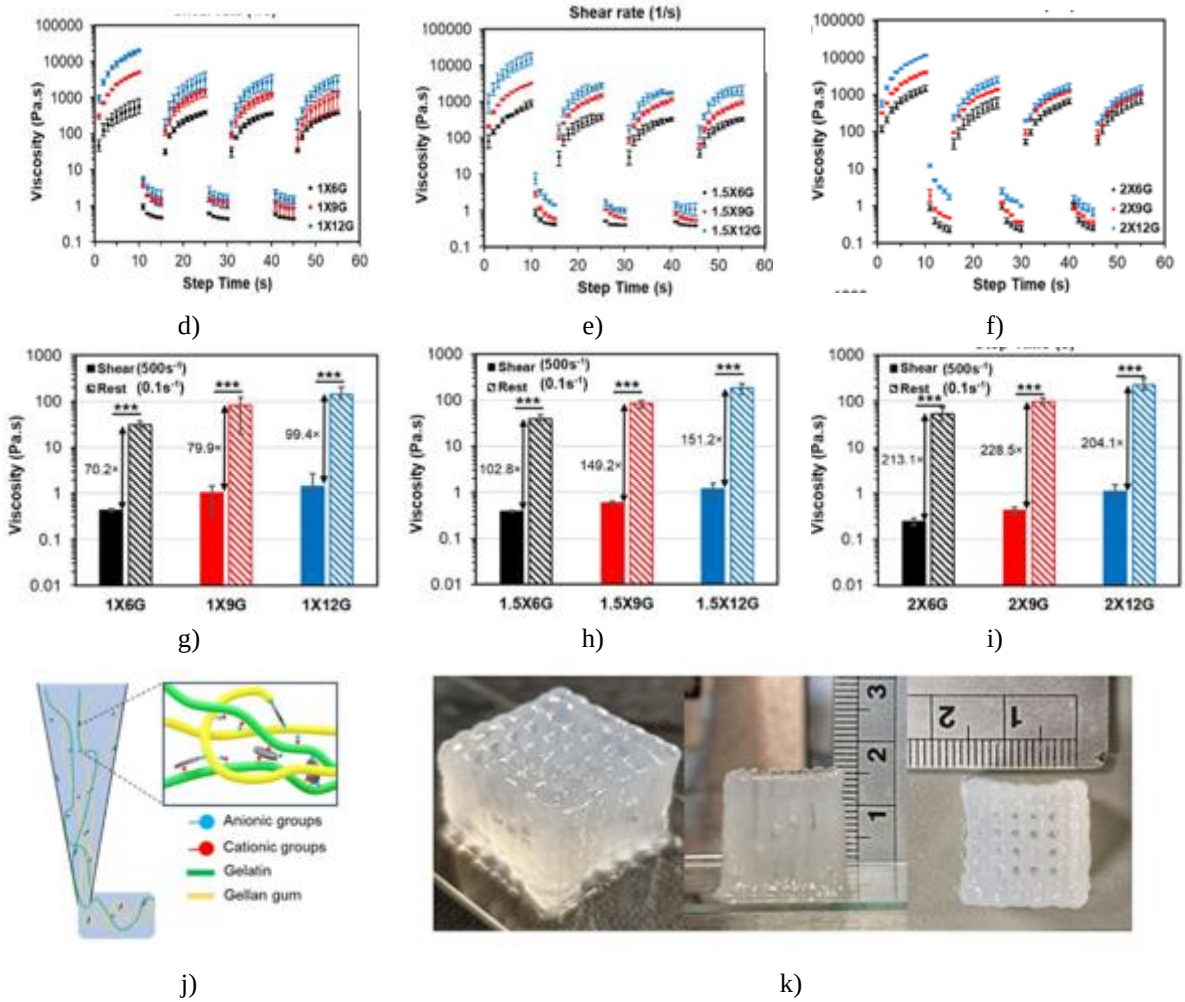


**Figure 2.** Rheological evaluation of composite Gel-X bio-inks. Effect of gelatin and Laponite XLG content on (a–c) viscosity profiles, (d–f) thixotropic response, and (g–i) structural recoverability. (j) Schematic depiction of intermolecular associations within the Gel-X network. (k) 3D bioprinted grid constructs (15 × 15 × 15 mm) displaying excellent shape retention.

Thixotropy and recovery were further examined through repeated shear-rest cycles designed to replicate the intermittent flow conditions of layer-by-layer deposition. The tests showed that Gel-X bio-inks recovered viscosity promptly when shifting from high shear (500 $s^{-1}$) to low shear (0.1 $s^{-1}$) across three successive cycles **(Figures 2d–2f)**. Earlier research has indicated that Laponite-containing systems can return to a gel state in as little as ~0.08 s following shear removal [56]. Quantitative assessment of recovery revealed that higher Laponite XLG loadings markedly enhanced restoration: recovery ratios rose from 70.2–99.4× at 1.0% Laponite XLG to 102.8–151.2× at 1.5% and 204.1–228.5× at 2.0% **(Figures 2g–2i)**. These results underscore the important contribution of Laponite XLG to shape maintenance during printing.

The amphoteric surface charge of Laponite XLG facilitates interactions with both positively and negatively charged segments of gelatin and gellan gum, generating a strong yet readily flowable network suited to bioprinting **(Figure 2j)**. The practical printability of these inks was illustrated by the successful fabrication of grid structures (15 × 15 × 15 mm) using 27G needles (inner diameter 210 μm). Rapid viscosity recovery enabled the construction of freestanding features reaching 1.5 mm in height **(Figure 2k)**.

*Microstructure analysis of Gel-X bio-inks*

To elucidate the internal organization resulting from polymer interactions, the microstructure of the various Gel-X formulations was visualized by FE-SEM **(Figure 3a)**. Quantitative ImageJ analysis indicated that porosity tended to decline as gelatin concentration increased. Raising gelatin content from 6% w/v to 12% w/v reduced porosity from approximately 41.5–50.1% to 23.6–30.2% **(Figure 3b)**. A parallel reduction occurred in pore size, decreasing from roughly 49.4–60.7 nm to 29.5–45.8 nm **(Figure 3c)**. These changes are ascribed to the formation

of a more compact polymer network at higher gelatin levels, which limits interstitial space and may potentially restrict nutrient transport to encapsulated cells.

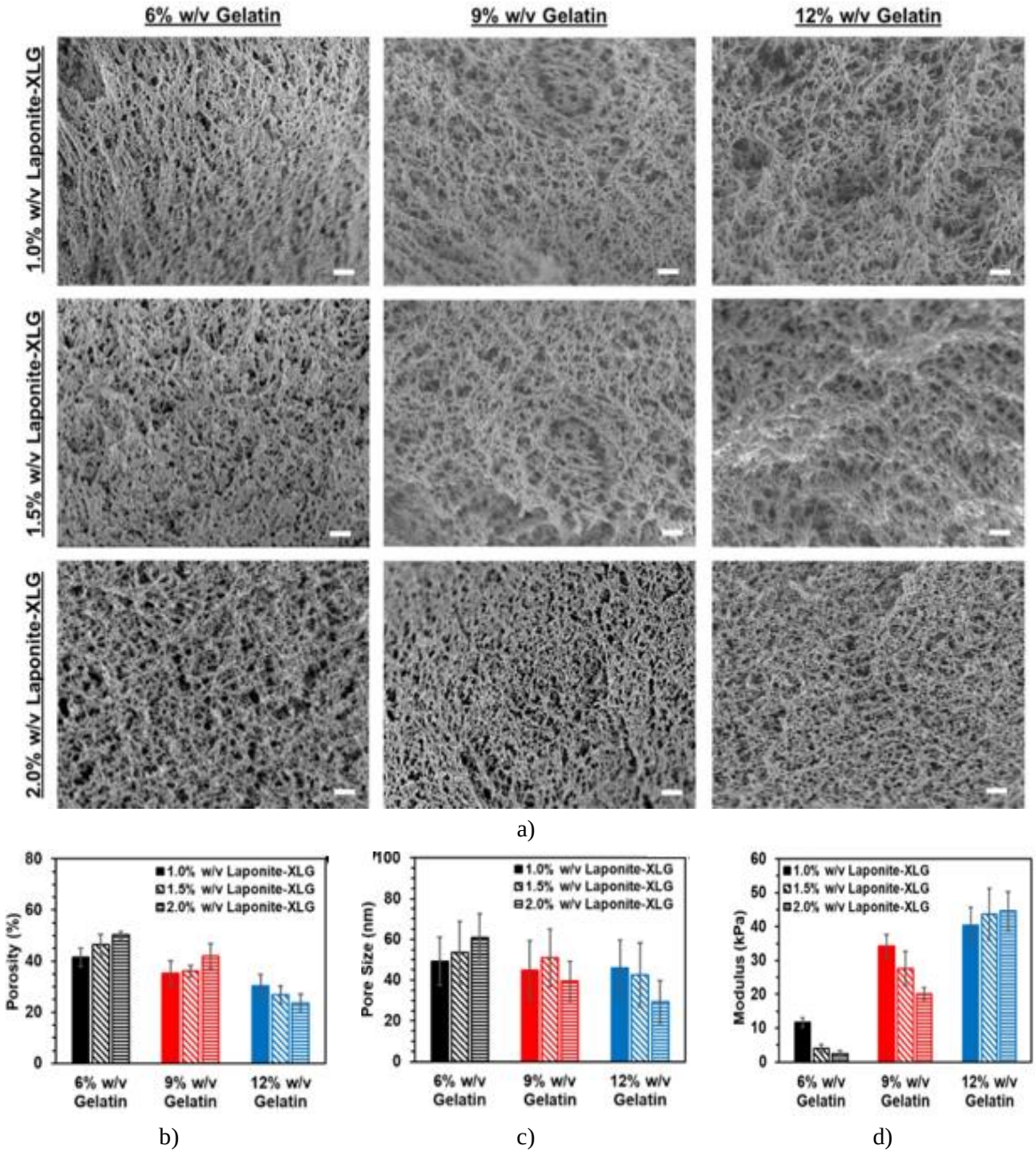


**Figure 3.** (a) Field-emission scanning electron microscopy (FE-SEM) micrographs of composite Gel-X bio-inks captured at 30,000× magnification (scale bar = 250 nm), illustrating microstructural variations with different gelatin and Laponite XLG levels. Quantitative assessment of (b) porosity and (c) pore size in relation to gelatin and Laponite XLG concentrations. (d) Compressive modulus data demonstrating enhanced stiffness at elevated gelatin and Laponite XLG contents, improving overall structural support.

In formulations with 6% w/v gelatin, higher Laponite XLG content increased pH and shifted the net charge of gelatin from positive (in 1X6G) to negative (in 1.5X6G and 2X6G). This charge reversal induced greater turbidity due to electrostatic repulsion between similarly charged gelatin and gellan gum chains at elevated pH. The resulting polymer aggregation diminished dispersion stability, producing higher porosity and enlarged pores with increasing Laponite XLG. This was corroborated by compression testing, which showed reduced compressive modulus at higher Laponite XLG loadings, consistent with a less densely packed structure **(Figure 3d)**.

For bio-inks containing 9% w/v gelatin, progressive addition of Laponite XLG raised pH and diminished the net positive charge on gelatin, thereby weakening attractive ionic forces. Consequently, porosity increased. Pore size initially expanded with rising Laponite XLG, reaching a maximum at 1.5% w/v before contracting at 2.0% w/v. At the highest Laponite concentration, the dense arrangement of disc-shaped nanoparticles appeared to strengthen interactions among gelatin and gellan gum, leading to tighter packing and smaller pores. Nevertheless, compressive modulus values generally declined with increased Laponite XLG, indicating reduced network cohesion **(Figure 3d)**.

In the case of 12% w/v gelatin formulations, pH values stayed within a mildly acidic to neutral range (pH 6.5–7.0), maintaining a stronger net positive charge on gelatin. This enhanced electrostatic attraction to negatively charged Laponite XLG produced a more compact matrix, manifested as lower porosity and smaller pore dimensions with rising Laponite content. Compression results supported this trend, revealing higher modulus values at elevated Laponite XLG concentrations and confirming improved structural reinforcement **(Figure 3d)**.

*Thermal stability and degradation studies of Gel-X bio-inks*

One of the primary drawbacks of gelatin-based bio-inks in their unmodified state is insufficient thermal resistance near body temperature (~37°C), which severely constrains their use in tissue engineering. Temperature sweep tests performed on control samples of pure gelatin (6%, 9%, and 12% w/v) identified crossover temperatures—where storage modulus (G′) equals loss modulus (G″)—at 26.22°C, 29.09°C, and 34.01°C, respectively **(Figure 4a)**. These transition points signify the change from a predominantly elastic to a viscous state, revealing the thermal weakness of unmodified gelatin under physiological conditions.

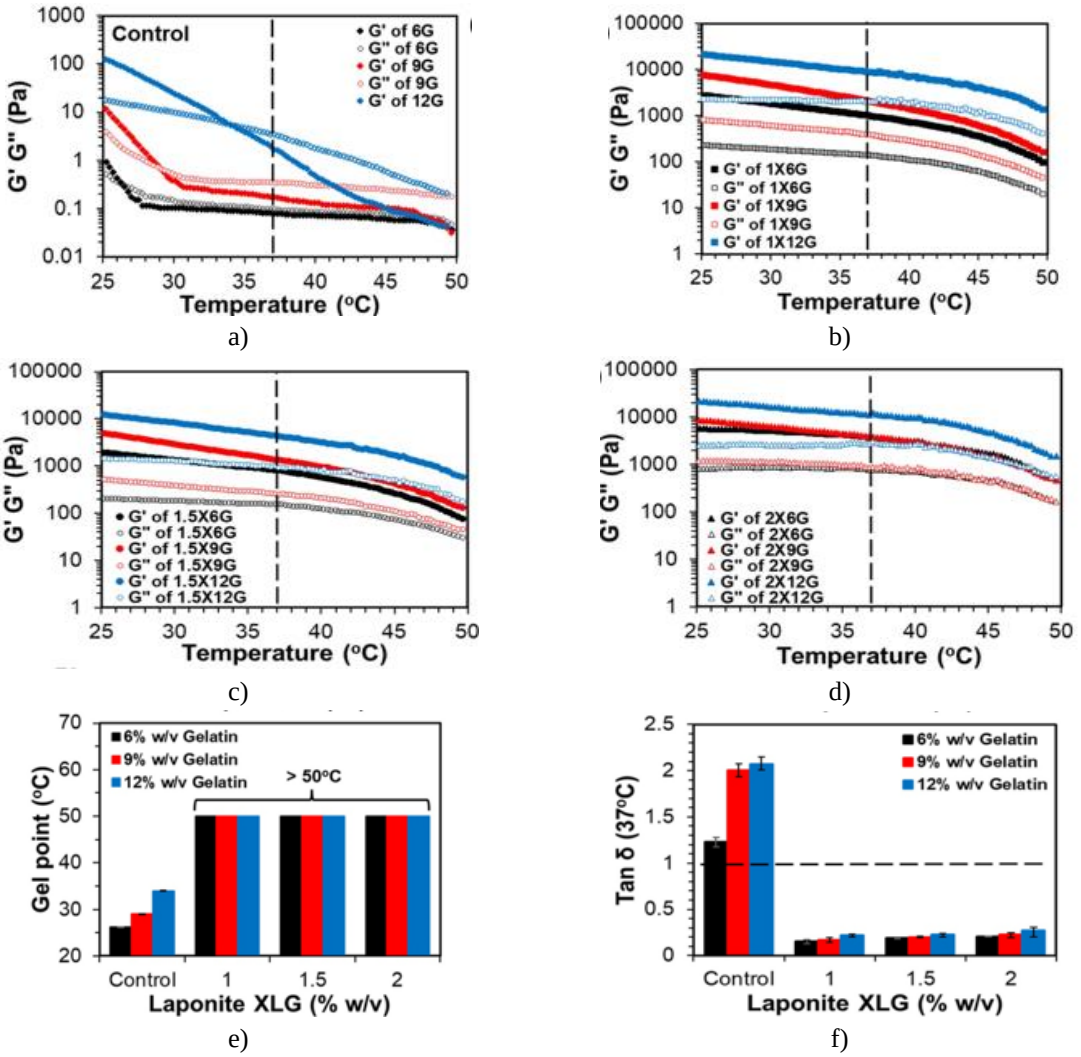


**Figure 4.** Temperature effects on the rheological characteristics of composite Gel-X bio-inks. Storage (G′) and loss (G″) moduli for gelatin-gellan gum systems reinforced with different Laponite XLG levels: (a)

unreinforced control, (b) 1.0% w/v Laponite XLG, (c) 1.5% w/v Laponite XLG, and (d) 2.0% w/v Laponite XLG. The vertical dotted line marks physiological temperature (37°C). (e) Variation of tan δ (G″/G′) at 37°C as a function of Laponite XLG and gelatin content. (f) Gel points recorded for the laponite-reinforced gelatin-gellan gum formulations under different compositions.

By comparison, all composite Gel-X formulations lacked crossover points throughout the temperature sweep **(Figures 4b–4d)**, demonstrating markedly superior thermal endurance. This advancement stems from the cooperative reinforcement provided by Laponite XLG nanoclay and gellan gum. The latter establishes an interpenetrating network with gelatin, while the nanoclay introduces additional physical crosslinks and structural support, shifting the gelation temperature beyond 50°C **(Figure 4e)**. As a result, the composites maintain robust mechanical performance at physiological temperatures, supporting their application in cell-laden constructs. Analysis of the damping factor (tan δ) further confirmed these improvements. Pure gelatin controls exhibited tan δ values exceeding 1 (1.23 for 6%, 2.00 for 9%, and 2.07 for 12% w/v) at 37°C, indicating viscous dominance. In contrast, Gel-X samples yielded tan δ values between 0.17 and 0.30 **(Figure 4f)**, confirming a transition to elastic, gel-like behavior after incorporation of the nanoclay and gellan gum.

Long-term stability was assessed through degradation experiments spanning 14 days. Pure gelatin specimens dissolved entirely within the first hour, highlighting their rapid breakdown and limited practical value without additives. The reinforced Gel-X bio-inks, however, showed considerably slower degradation rates, with both mass and volume retention increasing alongside higher Laponite XLG content. This protective effect arises from the creation of a tightly interconnected network that impedes hydrolytic processes. While elevated gelatin levels initially enhanced water uptake and swelling, nanoclay concentration was the dominant factor governing sustained integrity. After 14 days, mass retention for 1% Laponite XLG groups was 60.1 ± 1.26% (1X6G), 63.0 ± 2.17% (1X9G), and 64.1 ± 1.85% (1×12G) **(Figure 5a)**. At 1.5% Laponite XLG, retention improved to 67.6 ± 2.08% (1.5X6G), 70.8 ± 0.93% (1.5X9G), and 73.4 ± 0.64% (1.5×12G) **(Figure 5b)**. The 2% Laponite XLG series achieved the highest values: 74.9 ± 2.55% (2X6G), 76.8 ± 2.37% (2X9G), and 79.1 ± 3.41% (2×12G) **(Figure 5c)**. Volume retention displayed analogous trends, ranging from 73.4–80.3% (1X series), 76.0–82.1% (1.5X series), and 78.9–85.0% (2X series) **(Figures 5c–5f)**. Collectively, these data illustrate a controlled, gradual degradation pattern in Gel-X bio-inks that plateaus by day 14 **(Figure 5g)**. The favorable combination of slow resorption, thermal resilience, and mechanical durability underscores their suitability for tissue culture and various biomedical purposes.

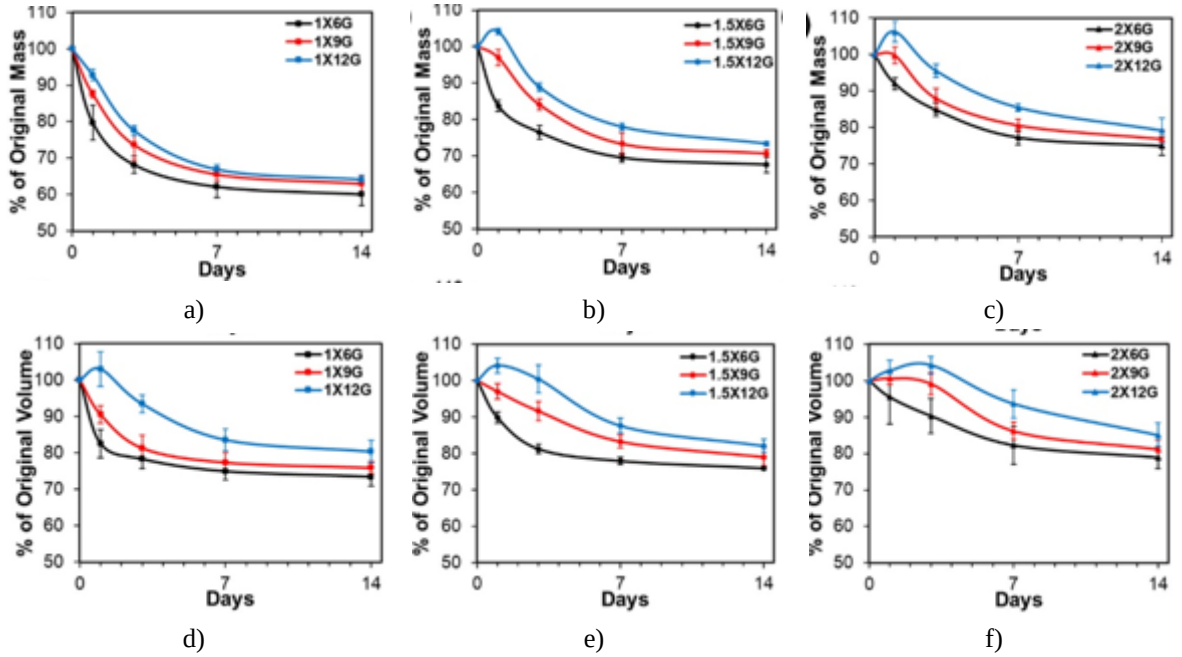

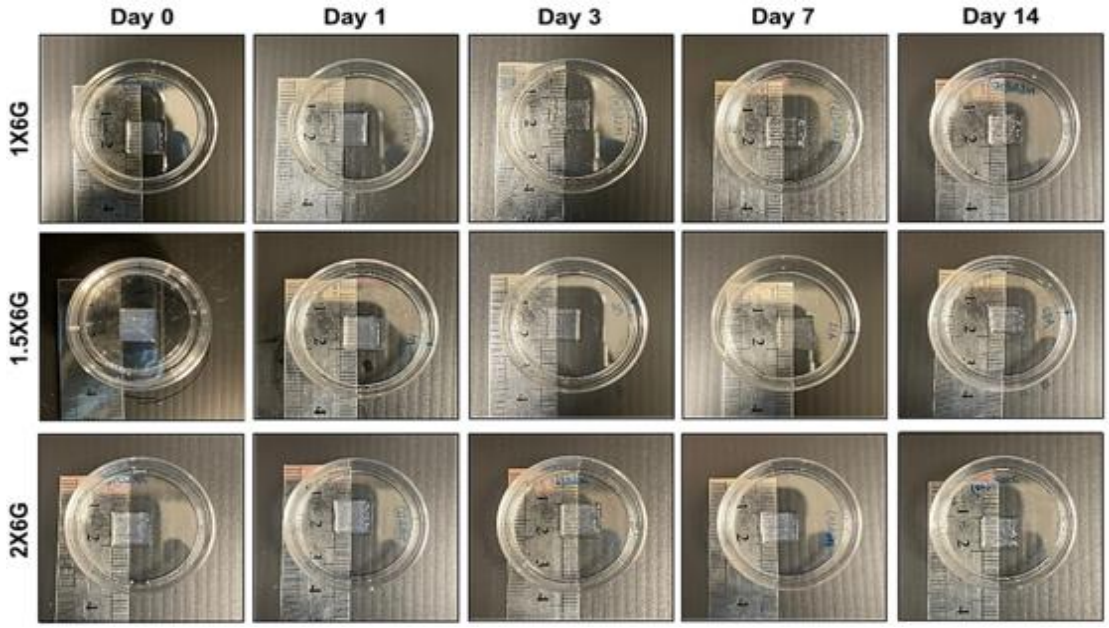


g)

**Figure 5.** Degradation kinetics of composite Gel-X bio-inks monitored over 14 days. Percentage alterations in (a–c) initial mass and (d–f) initial volume for series containing 1.0% w/v (a, d), 1.5% w/v (b, e), and 2.0% w/v (c, f) Laponite XLG across varying gelatin loadings. (g) Photographs depicting macroscopic dimensional changes in printed Gel-X constructs at selected intervals.

*Multi-modal bioprinting of 3D tissue constructs*

Cell-containing 3D tissue constructs were generated from Gel-X bio-inks employing a hybrid multi-modal printing strategy designed to optimize both biological compatibility and mechanical performance. This technique merged extrusion of the Gel-X material with microvalve jetting of cell suspensions, enabling the layer-by-layer assembly of complex multicellular structures **(Figure 6a)**. Continuous Gel-X sheets were deposited as supportive bases, onto which cell-laden droplets were precisely jetted, with the cycle repeated to build the final multilayered constructs. The integration of extrusion and jetting modalities effectively mitigates issues inherent to extrusion printing alone, notably the challenge of achieving uniform cell distribution within viscous inks.

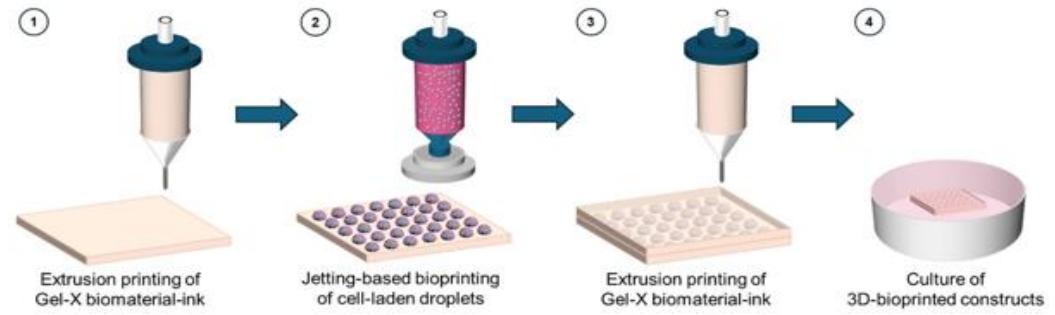


a)

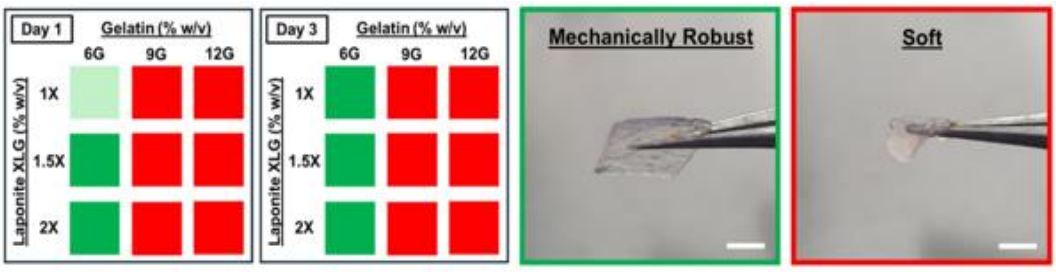


b)

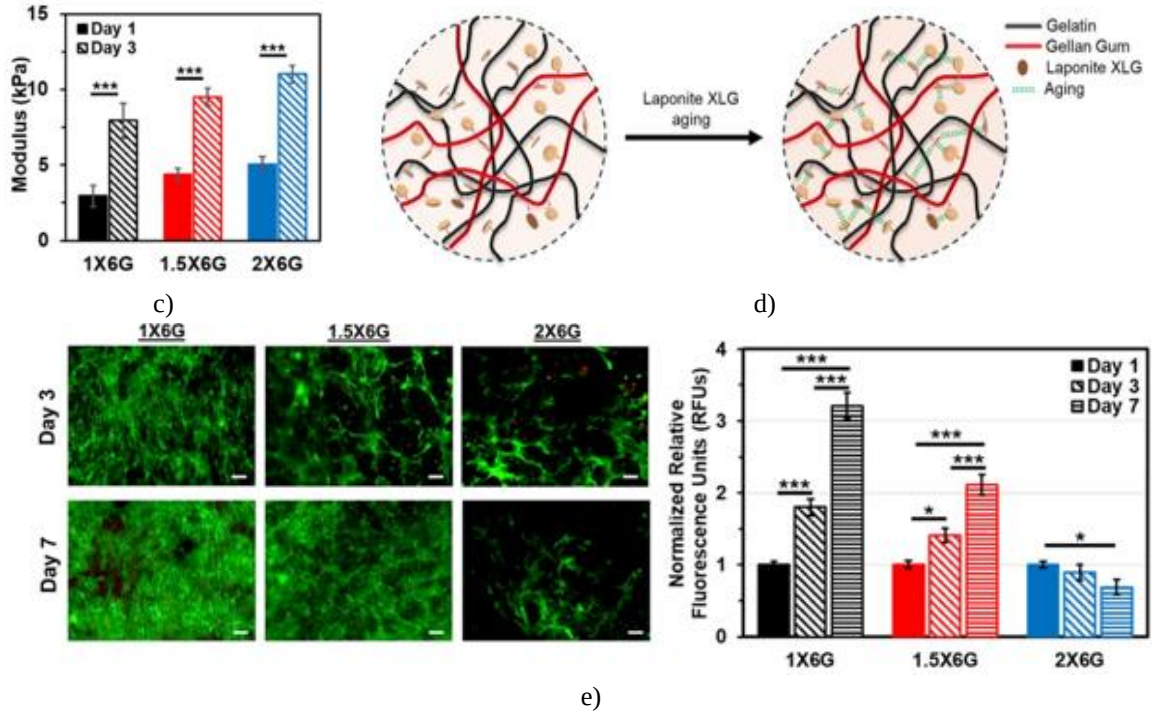


**Figure 6.** (a) Schematic of multi-modal bioprinting workflow for 3D cell-laden tissue constructs: extrusion of Gel-X bio-ink combined with jetting of cell suspensions, repeated sequentially to form complete structures. (b) Assessment of mechanical robustness on Day 1 and Day 3 via forceps lift test (green denotes stable constructs; red denotes mechanically weak samples), scale bar = 1 cm. (c) Quantitative compressive modulus values obtained from uniaxial testing of the printed constructs. (d) Illustration of progressive ageing in Laponite XLG nanoclay, leading to elevated modulus over time. (e) Cell proliferation profile measured by normalized relative fluorescence units (RFUs) using the PrestoBlue® assay, with corresponding live/dead fluorescence micrographs at Days 1, 3, and 7, scale bar = 100 µm. Data represent mean ± standard deviation, n = 5, ***$p < 0.001$ and *$p < 0.05$.

The structural durability of the printed cell-laden 3D constructs was evaluated qualitatively through a forceps lift test conducted on Days 1 and 3 **(Figure 6b)**. Samples prepared with elevated gelatin levels (9% and 12% w/v) generally remained pliable and tended to collapse under self-weight. This outcome relates to the pronounced water-attracting nature of gelatin chains, which drives extensive hydration and expansion (Supporting Information S1). These results were consistent with the degradation experiments, where 6% w/v gelatin-based constructs (1X6G: 79.7% mass retention and 82.5% volume retention; 1.5X6G: 83.8% mass retention and 89.8% volume retention; 2X6G: 92.0% mass retention and 95.5% volume retention) showed no evidence of swelling. In comparison, constructs with 9% and 12% gelatin typically displayed swelling on Day 1, evidenced by gains in both mass and volume. Notably, the 1X6G group exhibited better handling strength by Day 3.

Uniaxial compression tests provided quantitative confirmation of time-dependent stiffening. The compressive modulus increased from 2.95 ± 0.68 kPa to 7.94 ± 0.53 kPa for 1X6G, from 4.38 ± 1.17 kPa to 9.51 ± 1.71 kPa for 1.5X6G, and from 5.06 ± 1.09 kPa to 11.03 ± 2.86 kPa for 2X6G **(Figure 6c)**. This progressive enhancement may partly stem from the natural ageing of Laponite [60-62], during which the disc-shaped nanoparticles reorganize into a thermodynamically favored configuration that strengthens the gel network **(Figure 6d)**. The culture medium's ionic composition further promotes this process by reducing electrostatic repulsion between platelets and accelerating gelation. Cations in the medium also support ionic crosslinking of gellan gum, collectively bolstering the mechanical stability of the printed material.

Cell growth within the constructs was tracked using the PrestoBlue® metabolic assay, measuring normalized relative fluorescence units (RFUs) at Days 1, 3, and 7. Fibroblasts in the 1X6G and 1.5X6G groups continued to proliferate steadily and adopted elongated shapes **(Figure 6e)**. However, the 2X6G group showed a decline in normalized RFUs over the same period, even though cell morphology remained elongated. This reduction may arise from ion release at higher Laponite concentrations, which can exert cytotoxic effects. Additionally, overly rigid matrices may impose mechanical constraints on the embedded cells, impairing their function. While

literature generally recommends Laponite concentrations ≤2% w/v to ensure good cell survival [63-66], some cell lineages such as preosteoblasts and bone marrow mesenchymal stem cells have demonstrated tolerance to concentrations as high as 6–8% w/v [67, 68].

Overall, the Gel-X bio-inks offer strong mechanical properties, favorable thermal resistance, and controllable degradation rates, making them promising for tissue engineering cultures. Nevertheless, Laponite content must be carefully adjusted to harmonize mechanical performance with cell compatibility. These observations underscore the need for bio-ink designs tailored to specific cellular demands, thereby supporting wider adoption in sophisticated bioprinting platforms.

## Conclusion

This study presents an economical and sustainable physically crosslinked gelatin-based bio-ink (Gel-X) formulated from gelatin, Laponite XLG nanoclay, gellan gum, and sucrose. The resulting material displays markedly improved printability, structural stability, and resistance to breakdown. Its straightforward aqueous preparation and use of low-cost ingredients render Gel-X highly accessible for multi-modal bioprinting strategies. The workflow successfully combines extrusion of the bio-ink with jetting of cell suspensions to construct multilayered cell-laden 3D structures in a sequential manner. Detailed rheological investigations confirmed smooth flow during extrusion and efficient structural recovery, enabling accurate fabrication.

It is important to acknowledge that porcine Type A gelatin was used throughout; other gelatin types with differing isoelectric points, amino acid profiles, or production methods may yield different outcomes. Future work should investigate alternative sources to expand versatility and accommodate various ethical or cultural considerations. In summary, Gel-X bio-inks effectively address longstanding limitations in printability, mechanical strength, and physiological stability without relying on complex chemical modifications. Continued development of sustainable gelatin substitutes is likely to accelerate the transition of bioprinting technologies from research settings toward clinical implementation.

**Acknowledgments:** None

**Conflict of Interest:** None

**Financial Support:** None

**Ethics Statement:** None

## References

1. Chua CK, An J, Fan S, Zhang X, Ouyang L, Liu H, et al. A perspective on transformative bioprinting. Int J Bioprint. 2025;11:1.
2. Ng WL, An J, Chua CK. Process, material, and regulatory considerations for 3D printed medical devices and tissue constructs. Engineering. 2024;36:146-66.
3. Shapira A, Dvir T. 3D tissue and organ printing—Hope and reality. Adv Sci (Weinh). 2021;8(10):2003751.
4. Ng WL, Chua CK, Shen YF. Print me an organ! Why we are not there yet. Prog Polym Sci. 2019;97:101145.
5. Bejleri D, Streeter BW, Nachlas ALY, Brown ME, Gaetani R, Christman KL, et al. A bioprinted cardiac patch composed of cardiac-specific extracellular matrix and progenitor cells for heart repair. Adv Healthc Mater. 2018;7(23):e1800672.
6. Noor N, Shapira A, Edri R, Gal I, Wertheim L, Dvir T. 3D printing of personalized thick and perfusable cardiac patches and hearts. Adv Sci (Weinh). 2019;6:1900344.
7. Liu J, Miller K, Ma X, Dewan S, Lawrence N, Whang G, et al. Direct 3D bioprinting of cardiac micro-tissues mimicking native myocardium. Biomaterials. 2020;256:120204.
8. Flégeau K, Puiggali-Jou A, Zenobi-Wong M. Cartilage tissue engineering by extrusion bioprinting utilizing porous hyaluronic acid microgel bioinks. Biofabrication. 2022;14(3):034105.
9. Wang Y, Pereira RF, Peach C, Huang B, Vyas C, Bartolo P. Robotic in situ bioprinting for cartilage tissue engineering. Int J Extrem Manuf. 2023;5:032004.

10. Puiggalí-Jou A, Rizzo R, Bonato A, Fisch P, Ponta S, Weber DM, et al. Flight biofabrication supports maturation of articular cartilage with anisotropic properties. Adv Healthc Mater. 2024;13(12):e2302179.
11. Isaacson A, Swioklo S, Connon CJ. 3D bioprinting of a corneal stroma equivalent. Exp Eye Res. 2018;173:188-93.
12. Sorkio A, Koch L, Koivusalo L, Deiwick A, Miettinen S, Chichkov B, et al. Human stem cell based corneal tissue mimicking structures using laser-assisted 3D bioprinting and functional bioinks. Biomaterials. 2018;171:57-71.
13. Mörö A, Samanta S, Honkamäki L, Rangasami VK, Puistola P, Kauppila M, et al. Hyaluronic acid based next generation bioink for 3D bioprinting of human stem cell derived corneal stromal model with innervation. Biofabrication. 2022;15(1):015020.
14. Fan P, Jin F, Qin Y, Wu Y, Yang Q, Liu H, et al. Multiscale 3D bioprinting for the recapitulation of lung tissue. Int J Bioprint. 2023;9(6):1166.
15. Kang D, Park JA, Kim W, Kim S, Lee HR, Kim WJ, et al. All-inkjet-printed 3D alveolar barrier model with physiologically relevant microarchitecture. Adv Sci (Weinh). 2021;8:2004990.
16. Ng WL, Ayi TC, Liu Y-C, Sing SL, Yeong WY, Tan B-H. Fabrication and characterization of 3D bioprinted triple-layered human alveolar lung models. Int J Bioprint. 2021;7(2):332. doi:10.18063/ijb.v7i2.332
17. Ng WL, Tan ZQ, Yeong WY, Naing MW. Proof-of-concept: 3D bioprinting of pigmented human skin constructs. Biofabrication. 201;10(2):025005. doi:10.1088/1758-5090/aa9e1e
18. Zhang Y, Enhejirigala, Yao B, Li Z, Song W, Li J, et al. Using bioprinting and spheroid culture to create a skin model with sweat glands and hair follicles. Burns Trauma. 2021;9:tkab013. doi:10.1093/burnst/tkab013
19. Ng WL, Wang S, Yeong WY, Naing MW. Skin bioprinting: impending reality or fantasy? Trends Biotechnol. 2016;34:689-99. doi:10.1016/j.tibtech.2016.04.006
20. Ramesh S, Harrysson OLA, Rao PK, Tamayol A, Cormier DR, Zhang Y, et al. Extrusion bioprinting: Recent progress, challenges, and future opportunities. Bioprinting. 202; 2:e00116.
21. Fu Z, Naghieh S, Xu C, Wang C, Sun W, Chen X. Printability in extrusion bioprinting. Biofabrication. 202;13:033001. doi:10.1088/1758-5090/abe7ab
22. Naghieh S, Chen X. Printability-a key issue in extrusion-based bioprinting. J Pharm Anal. 2021;11:564-79. doi:10.1016/j.jpha.2021.02.001
23. Ng WL, Shkolnikov V. Jetting-based bioprinting: process, dispense physics, and applications. Bio-des Manuf. 2024;7:771-99.
24. Ng WL, Lee JM, Yeong WY, Naing MW. Microvalve-based bioprinting - process, bio-inks and applications. Biomater Sci. 2017;5:632-47. doi:10.1039/c6bm00861e
25. Suntornnond R, Ng WL, Shkolnikov V, Yeong WY. A facile method to fabricate cell-laden hydrogel microparticles of tunable sizes using thermal inkjet bioprinting. Droplet. 2024;3:e144. doi:10.1002/dro2.144
26. Ng WL, Lee JM, Zhou M, Chen Y-W, Lee K-XA, Yeong WY, et al. Vat polymerization-based bioprinting-process, materials, applications and regulatory challenges. Biofabrication. 2020;12:022001. doi:10.1088/1758-5090/ab6034
27. Li W, Mille LS, Robledo JA, Uribe T, Huerta V, Zhang YS. Recent advances in formulating and processing biomaterial inks for vat polymerization-based 3D printing. Adv Healthcare Mater. 2020;9:2000156. doi:10.1002/adhm.202000156
28. Boularaoui S, Al Hussein G, Khan KA, Christoforou N, Stefanini C. An overview of extrusion-based bioprinting with a focus on induced shear stress and its effect on cell viability. Bioprinting. 2020;20:e00093.
29. Daly AC. Granular hydrogels in biofabrication: recent advances and future perspectives. Adv Healthc Mater. 2023;13(25):e2301388. doi:10.1002/adhm.202301388
30. Blaeser A, Duarte Campos DF, Puster U, Richtering W, Stevens MM, Fischer H. Controlling shear stress in 3D bioprinting is a key factor to balance printing resolution and stem cell integrity. Adv Healthc Mater. 2016;5:326-33. doi:10.1002/adhm.201500677
31. Ng WL, Huang X, Shkolnikov V, Goh GL, Suntornnond R, Yeong WY. Controlling droplet impact velocity and droplet volume: key factors to achieving high cell viability in sub-nanoliter droplet-based bioprinting. Int J Bioprint. 2022;8:424. doi:10.18063/ijb.v8i1.424
32. Ng WL, Huang X, Shkolnikov V, Suntornnond R, Yeong WY. Polyvinylpyrrolidone-based bioink: influence of bioink properties on printing performance and cell proliferation during inkjet-based bioprinting. Bio-des Manuf. 2023;6:676-90.

33. Ng WL, Shkolnikov V. Optimizing cell deposition for inkjet-based bioprinting. Int J Bioprint. 2024;10:2135. doi:10.36922/ijb.2135
34. Khandaker M, Orock A, Tarantini S, White J, Yasar O. Biomechanical performances of networked polyethylene glycol diacrylate: effect of photoinitiator concentration, temperature, and incubation time. Int J Biomater. 2016;2016:3208312. doi:10.1155/2016/3208312
35. Xu H, Casillas J, Krishnamoorthy S, Xu C. Effects of Irgacure 2959 and lithium phenyl-2,4,6-trimethylbenzoylphosphinate on cell viability, physical properties, and microstructure in 3D bioprinting of vascular-like constructs. Biomed Mater. 2020;15:055021. doi:10.1088/1748-605X/ab954e
36. Masuma R, Kashima S, Kurasaki M, Okuno T. Effects of UV wavelength on cell damages caused by UV irradiation in PC12 cells. J Photochem Photobiol B Biol. 2013;125:202-8.
37. Xu T, Binder KW, Albanna MZ, Dice D, Zhao W, Yoo JJ, et al. Hybrid printing of mechanically and biologically improved constructs for cartilage tissue engineering applications. Biofabrication. 2013;5:015001. doi:10.1088/1758-5082/5/1/015001
38. Daly AC, Kelly DJ. Biofabrication of spatially organised tissues by directing the growth of cellular spheroids within 3D printed polymeric microchambers. Biomaterials. 2019;197:194-206.
39. Abellan Lopez M, Hutter L, Pagin E, Vélier M, Véran J, Giraudo L, et al. In vivo efficacy proof of concept of a large-size bioprinted dermo-epidermal substitute for permanent wound coverage. Front Bioeng Biotechnol. 2023;11:1217655. doi:10.3389/fbioe.2023.1217655
40. Gungor-Ozkerim PS, Inci I, Zhang YS, Khademhosseini A, Dokmeci MR. Bioinks for 3D bioprinting: an overview. Biomater Sci. 2018;6:915-46. doi:10.1039/c7bm00765e
41. Decante G, Costa JB, Silva-Correia J, Collins MN, Reis RL, Oliveira JM. Engineering bioinks for 3D bioprinting. Biofabrication. 2021;13:032001. doi:10.1088/1758-5090/abec2c
42. Ng WL, Lee JM, Zhou M, Yeong WY. Hydrogels for 3-D bioprinting-based tissue engineering. In: Rapid Prototyping of Biomaterials (Ed: R. Narayan). Elsevier; 2020 .p. 183-204.
43. Su J, Ng WL, An J, Yeong WY, Chua CK, Sing SL. Achieving sustainability by additive manufacturing: a state-of-the-art review and perspectives. Virtual Phys Prototyp. 2024;19:e2438899. doi:10.1080/17452759.2024.2438899
44. Asim S, Tabish TA, Liaqat U, Ozbolat IT, Rizwan M. Advances in gelatin bioinks to optimize bioprinted cell functions. Adv Healthc Mater. 2023;12:2203148. doi:10.1002/adhm.202203148
45. He J, Sun Y, Gao Q, He C, Yao K, Wang T, et al. Gelatin methacryloyl hydrogel, from standardization, performance, to biomedical application. Adv Healthc Mater. 2023;12:2300395. doi:10.1002/adhm.202300395
46. Yue K, Trujillo-de Santiago G, Alvarez MM, Tamayol A, Annabi N, Khademhosseini A. Synthesis, properties, and biomedical applications of gelatin methacryloyl (GelMA) hydrogels. Biomaterials. 2015;73:254-71. doi:10.1016/j.biomaterials.2015.08.045
47. Tan C-C, Karim AA, Uthumporn U, Ghazali FC. Effect extraction temperature on the emulsifying properties of gelatin from black tilapia (Oreochromis mossambicus) skin. Food Hydrocoll. 2020;108:106024.
48. Karim AA, Bhat R. Fish gelatin: properties, challenges, and prospects as an alternative to mammalian gelatins. Food Hydrocoll. 2009;23:563-76. doi:10.1016/j.foodhyd.2008.07.001
49. Yin YJ, Yao KD, Cheng GX, Ma JB. Properties of polyelectrolyte complex films of chitosan and gelatin. Polym Int. 1999;48:429-32. doi:10.1002/(SICI)1097-0126(199906)48:6<429::AID-PI160>3.0.CO;2-1
50. Gioffredi E, Boffito M, Calzone S, Giannitelli SM, Rainer A, Trombetta M, et al. Pluronic F127 hydrogel characterization and biofabrication in cellularized constructs for tissue engineering applications. Proced CIRP. 2016;49:125-32.
51. Ng WL, Yeong WY, Naing MW. Polyelectrolyte gelatin-chitosan hydrogel optimized for 3D bioprinting in skin tissue engineering. Int J Bioprint. 2016;2:53-62. doi:10.18063/IJB.2016.01.009
52. Koivisto JT, Gering C, Karvinen J, Cherian RM, Belay B, Hyttinen J, et al. Mechanically biomimetic gelatin-gellan gum hydrogels for 3D culture of beating human cardiomyocytes. ACS Appl Mater Interfaces. 2019;11:20589-602. doi:10.1021/acsami.8b22343
53. Lee KY, Shim J, Lee HG. Mechanical properties of gellan and gelatin composite films. Carbohydr Polym. 2004;56:251-4.

54. Gaharwar AK, Cross LM, Peak CW, Gold K, Carrow JK, Brokesh A, et al. 2D nanoclay for biomedical applications: regenerative medicine, therapeutic delivery, and additive manufacturing. Adv Mater. 2019;31:1900332. doi:10.1002/adma.201900332
55. Davern JW, Hipwood L, Bray LJ, Meinert C, Klein TJ. Addition of laponite to gelatin methacryloyl bioinks improves the rheological properties and printability to create mechanically tailorable cell culture matrices. APL Bioeng. 2024;8:016101. doi:10.1063/5.0166206
56. Jin Y, Liu C, Chai W, Compaan A, Huang Y. Self-supporting nanoclay as internal scaffold material for direct printing of soft hydrogel composite structures in air. ACS Appl Mater Interfaces. 2017;9:17456-65. doi:10.1021/acsami.7b03613
57. Ng WL, Yeong WY, Naing MW. Polyvinylpyrrolidone-based bio-ink improves cell viability and homogeneity during drop-on-demand printing. Materials. 2017;10:190. doi:10.3390/ma10020190
58. Zheng Y, Liang Y, Zhang D, Sun X, Liang L, Li J, et al. Gelatin-based hydrogels blended with gellan as an injectable wound dressing. ACS Omega. 2018;3:4766-75. doi:10.1021/acsomega.8b00308
59. Jatav S, Joshi YM. Chemical stability of Laponite in aqueous media. Appl Clay Sci. 2014;97:72-7.
60. Ruzicka B, Zaccarelli E, Zulian L, Angelini R, Sztucki M, Moussaïd A, et al. Observation of empty liquids and equilibrium gels in a colloidal clay. Nat Mater. 2011;10:56-60.
61. Joshi YM, Patel S, Suman K. Aqueous Laponite dispersions are attractive gels, not repulsive Wigner glasses: a critical commentary. J Rheol. 2024;68:145.
62. Dávila JL, d'Ávila MA. Laponite as a rheology modifier of alginate solutions: physical gelation and aging evolution. Carbohydr Polym. 2017;157:1-8. doi:10.1016/j.carbpol.2016.09.057
63. de Barros NR, Gomez A, Ermis M, Falcone N, Haghniaz R, Young P, et al. Gelatin methacryloyl and Laponite bioink for 3D bioprinted organotypic tumor modeling. Biofabrication. 2023;15:045005. doi:10.1088/1758-5090/ace0db
64. Cidonio G, Alcala-Orozco CR, Lim KS, Glinka M, Mutreja I, Kim YH, et al. Osteogenic and angiogenic tissue formation in high fidelity nanocomposite Laponite-gelatin bioinks. Biofabrication. 2019;11:035027. doi:10.1088/1758-5090/ab19fd
65. Ma Z, He H, Deng C, Ren Y, Lu D, Li W, et al. 3D bioprinting of proangiogenic constructs with induced immunomodulatory microenvironments through a dual cross-linking procedure using laponite incorporated bioink. Compos Part B Eng. 2022;229:109399.
66. Miao S, Zhou J, Liu B, Lei X, Wang T, Hao X, et al. A 3D bioprinted nano-laponite hydrogel construct promotes osteogenesis by activating PI3K/AKT signaling pathway. Mater Today Bio. 2022;16:100342.
67. Dong L, Bu Z, Xiong Y, Zhang H, Fang J, Hu H, et al. Facile extrusion 3D printing of gelatine methacrylate/Laponite nanocomposite hydrogel with high concentration nanoclay for bone tissue regeneration. Int J Biol Macromol. 2021;188:72-82. doi:10.1016/j.ijbiomac.2021.07.199
68. Wilson SA, Cross LM, Peak CW, Gaharwar AK. Shear-thinning and thermo-reversible nanoengineered inks for 3D bioprinting. ACS Appl Mater Interfaces. 2017;9:43449-58. doi:10.1021/acsami.7b13602